

https://dspace.org/

High room temperature coercivity from Fe2O3 nanoparticles embedded in silica

C.J. Masina; A.E. Chithwayo; T. Moyo; S Dlamini; Daniel Wamwangi

ELSEVIER SCIENCE BV
https://hdl.handle.net/10539/42115
WOS

Downloaded from a DSpace repository. https://dspace.org/

Journal of Magnetism and Magnetic Materials 610 (2024) 172521



Contents lists available at ScienceDirect

Journal of Magnetism and Magnetic Materials

journal homepage: www.elsevier.com/locate/jmmm



Research article

High room temperature coercivity from α-Fe_2O_3 nanoparticles embedded in silica

C.J. Masina [a,*], A.E. Chithwayo [a], T. Moyo [b], S. Dlamini [b], D. Wamwangi [c]

[a] School of Chemistry & Physics, University of KwaZulu-Natal, Pietermaritzburg Campus, Private Bag X01, Scottsville 3209, South Africa
[b] School of Chemistry & Physics, University of KwaZulu-Natal, Westville Campus, Private Bag X54001, Durban 4000, South Africa
[c] School of Physics, University of the Witwatersrand, East Campus, 1 Jan Smuts Ave, Braamfontein, South Africa

ARTICLE INFO

Keywords:
Hematite nanoparticles
High coercivity
Magnetic properties

ABSTRACT

Hematite (α-Fe_2O_3) nanoparticles embedded in SiO_2 matrix have been synthesized using Sol–gel method at 1100 °C to investigate the correlation between structural and magnetic properties. X-ray diffraction analysis revealed the formation of a single phase hematite in silica matrix (α-Fe_2O_3/ SiO_2). Transmission electron Microscopy has confirmed homogeneous spherical morphology of dimensions (118 +/- 28) nm. The room temperature Mössbauer spectroscopy revealed the weakly ferromagnetic state in the sample. The spectra was fitted with a model consisting of a single Lorentzian-shaped sextet with the Mössbauer parameters; the isomer shift of 0.37 mm/s, quadrupole shift of -0.10 mm/s, and the magnetic hyperfine field of 51.5 T. $M(H)$ magnetization curves (hysteresis loops) were recorded at 10, 100, 200 and 300 K for the sample. Room temperature magnetization measurements revealed a surprisingly high coercivity field of $H_C \sim 8.5$ kOe for the α-Fe_2O_3/ SiO_2 nanoparticles, and this was explained using the sub-particle structure model. A room temperature remanent magnetization of $M_r = 0.27$ emu/g and saturation magnetization $M_s = 1.90$ emu/g were recorded for this sample.

1. Introduction

Due to their unique magnetic properties, various magnetic nanomaterials have in recent years attracted attention, and among them is the iron (III) oxide hematite α-Fe_2O_3 [1–4]. Hematite is the most stable of the four polymorphs of Fe_2O_3 at ambient conditions [5]. Hematite nanoparticles have gained tremendous attention because they are effective and inexpensive materials for gas sensors, catalysis, and electrodes [6]. The magnetic properties of hematite are highly dependent on its nanoparticle size, morphology and microstructure [1,7–9]. Powell et al. [6] demonstrated that hematite with controlled nanoparticles size can undergo radiofrequency heating which makes them suitable for magnetic hyperthemia applications [6]. The magnetic properties of hematite in both bulk and as nanoparticles have been extensively studied in the past [2–5,10,11]. Bulk hematite presents a weak ferromagnetic (WF) or canted antiferromagnetic ordering below its Néel temperature $T_N = 950$ K due to Dzyaloshinskii–Moriya mechanism of the Fe^{3+} ion [5]. In this magnetic ordering, the magnetic moments of the two interpenetrating sublattices lies approximately in the basal plane. The magnetic moments in this configuration are not perfectly anti-parallel (see Fig. 1(a)), they are slightly canted (canting angle < 0.1°), which results in a weak ferromagnetic moment [12–14]. A canting angle of about 5° is also reported for this mineral [15,16]. Hematite undergoes a second magnetic phase transition from WF to antiferromagnetic (AFM) ordering at a transition temperature known as Morin transition temperature T_M, which commences at $T_M = 260$ K [2–5,10,11]. At T_M, the spins are reorientated by 90° (spin-flop transition) resulting in exactly antiparallel spin configuration along the c-axis (see Fig. 1 (b)) [14]. Thus, below T_M, hematite is considered an antiferromagnet and above T_M, it is considered a weak or canted antiferromagnet. It has been experimentally determined that the Morin transition temperature is particle size dependent i.e. T_M decreases with decreasing particle size and it is fully suppressed for particle sizes lesser than 20 nm [2,5,12,17]. The WF ordering in α-Fe_2O_3 has been suggested to be due to the result of both canted antiferromagnetism and from uncompensated spins [18,19].

The magnetic behavior of hematite is known to depend on the particle size, shape, and microstructure [2]. Depending on the particle size and microstructure of hematite, the coercivity field values has been reported by several studies to range from 0.3 to 5.2 kOe [20–23]. Additionally, studies by Rath et al. [8] and Bercoff & Bertorello [24] have reported high coercivity values from 4 to 6 kOe when temperature was raised up to room temperature. Chaudhari et al. [25] produced

* Corresponding author.
E-mail address: Masinac@ukzn.ac.za (C.J. Masina).

https://doi.org/10.1016/j.jmmm.2024.172521
Received 6 June 2024; Received in revised form 5 September 2024; Accepted 10 September 2024
Available online 14 September 2024
0304-8853/© 2024 The Authors. Published by Elsevier B.V. This is an open access article under the CC BY-NC-ND license (http://creativecommons.org/licenses/by-nc-nd/4.0/).

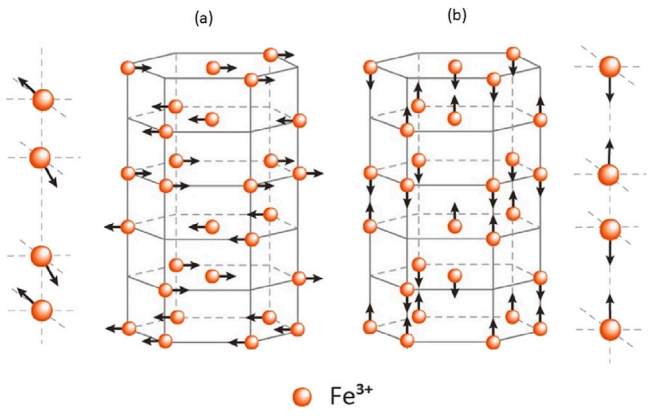

Fig. 1. Hematite crystal structure showing (a) Weakly ferromagnetic ordering ($T > T_M$) and (b) Antiferromagnetic ordering ($T < T_M$).
Source: Figure obtained from [14].

hematite superstructures with large coercivity values up to ~7 kOe. The large variability in these values is attributed in part to morphology, surface to volume ratio amongst other synthesis dependent process parameters and methods. The internal microstructure of hematite particles has also been highlighted as the origin for the observed high coercivities in hematite e.g. sub-particle structure was reported by Rath et al. [8] to be the reason for the observed high coercivity field in their study. Coating hematite with silica seems to have influence on coercivity e.g. Reufer et al. [26] reported an increase in coercivity of hematite nanoparticles as a result of silica coating. Tadic et al. [7] demonstrated that α-Fe_2O_3 nanoparticles in silica matrix can achieve coercivity of 4.3 kOe. It is worth mentioning that amongst the Fe_2O_3 polymorphs, the ε-Fe_2O_3 polymorph has shown the highest room temperature coercivity field of 20 kOe [27–29].

Hematite has shown microstructure-dependent magnetic properties, particularly coercivity [1,7,8]. In this present paper, we have investigated a new method to produce a hematite sample with high coercivity. α-Fe_2O_3 nanoparticles embedded in silica were synthesized by high temperature annealing using sol–gel method slightly modified from [30]. Here we report novel results on hematite nanoparticles exhibiting a high coercivity field of ~8.5 kOe at room temperature. According to our knowledge, this coercivity is the highest coercivity at room temperature reported for hematite nanoparticles.

2. Materials and methods

2.1. Synthesis of α-Fe_2O_3 nanoparticles

The α-Fe_2O_3/SiO_2 nanoparticles were prepared using a method sightly modified from García-Muñoz et al. [30]. The formation of the sol–gels between the modified and original methods were exactly the same. Briefly, A hydroethanolic solution of tetraethyl orthosilicate (TEOS) of molar composition, TEOS:Ethanol:water = 1:5:6 containing dissolved iron nitrate $Fe(NO_3)_3.9H_2O$ was prepared by adding 5.4 ml of distilled water and 26 ml of absolute ethanol were to a 100 ml beaker and stirred for few minutes. An amount of 10.60 g of $Fe(NO_3)_3.9H_2O$ was dissolved in the solution. The final step involved adding 20 ml of TEOS dropwise to the solution under stirring. The gelation process took 2 weeks to complete. But instead of annealing the sample in a stepwise manner i.e. from room temperature to 450 °C at a heating rate of 200 °C h^{-1} and then heated to 1100 °C at a heating rate of 80 °C h^{-1} and held there for 3 h, the sample in this project was only heated at 1100 °C for 3 h.

Bare α-Fe_2O_3 nanoparticles (not embedded in silica) were also synthesized and their magnetic properties were compared to that of the α-Fe_2O_3/SiO_2 sample. The sample was prepared using a sol–gel method previously reported by Zhang et al. [31]. A precursor solution was prepared by dissolving a known amount of $Fe(NO_3)_3$ in water, then citric acid was added. This was done according to the weight ratio between $Fe(NO_3)_3$ and citric acid of 0.5: 0.55. The mixture was refluxed at 70 °C for 30 min under continuous stirring to ensure a perfect homogeneity. The gel was obtained from the mixture by rotary evaporation and was heat treated at 525 °C for 3 h. A powder sample with crystallite size about 13 nm was obtained. The structural and morphological analysis of the sample were described in detail in Ref. [32].

2.2. Characterization

X-ray Diffraction: X-ray diffraction patterns were collected using a D8 Advance Bruker AXS X-ray diffractometer in the 2θ range of 20–80 at a step size of 0.034. For all measurements, the Cu-$K_{\alpha 1}$ line was used (λ = 1,5406 Å). The Lynx-eye detector operating as a position sensitive detector was used to record the diffraction pattern at 0.5 s/step. **Transmission Electron Microscopy**: The samples were analyzed by Transmission electron microscopy (TEM) using a JEOL JEM-1400 microscope operated at 200 kV. The Image J program was used to measure the particle size on the TEM images. **Mossbauer Spectroscopy**: The magnetic state of the samples were investigated using the Mossbauer spectroscopy. The Mossbauer spectra were acquired at room temperature using a conventional Mossbauer spectrometer with a ^{57}Co/Rh source for which calibration was done with a foil of metallic iron, the Mössbauer parameters are given relative to this standard at room temperature. The fitting of the data was carried out using Recoil Mössbauer analysis software and were fitted using the Lorentzian site analysis. **Vibrating Sample Magnetometer**: A vibrating sample magnetometer (VSM) operated in the DynaCool 12 T Physical Property Measurement System was used to collect isofield measurements at 300, 200, 100, and 10 K. The remanent magnetization (M_r) and coercivity H_c were studied using the isotherm and isofield conditions.

3. Results and discussion

3.1. Phase analysis & morphology

The phase composition of the sample was studied using powder X-ray diffraction (XRD) technique and Rietveld refinement was carried out using MAUD software for detailed structural analysis. The Rietveld refinement pattern of the α-Fe_2O_3 nanoparticles is presented in Fig. 2. The XRD profile of the sample shows the characteristic XRD peaks corresponding to planes (012), (104), (110), (113), (024), (116), (018),(214),(300), (119), (220), and (306). MAUD profile fitting shows that the structure of the sample is trigonal with space group R-3c:H and lattice parameters approximately a = 5.040(2) Å and c = 13.769(13) Å. The observed XRD reflections of the sample and calculated lattice parameters are consistent with previous reports [16,33,34] for a standard pattern of α-Fe_2O_3, an indication that the sample consist of only pure hematite phase. The average crystallite size and microstrain was estimated by using MAUD for the sample and are approximately 42 ± 2.0 and 0.001, respectively. The refinement parameters, goodness-of-fit (GoF) along with the weighted profile factor (R_{wp}) and Bragg factor (R_b) were used to assess the quality of the refinement. According to Kisi [35], a good refinement should meet the criteria of goodness-of-fit (GoF) < 4% and R_{wp} < 20%. For the refinement reported in Fig. 2, the GoF and R_{wp} were 3% and 18%, respectively.

The Williamson–Hall (W–H) method was also used to estimate the crystallite size and microstrain from the XRD profile of the sample. It is known that both the instrument and sample contributes to the total broadening (β_t) of the XRD peak. If the instrumental peak broadening is decoupled in the XRD reflection then the resultant broadening is associated purely to the sample, with contributions emerging from the crystallite size (β_D) and microstrain (β_ε). The broadening of the peak

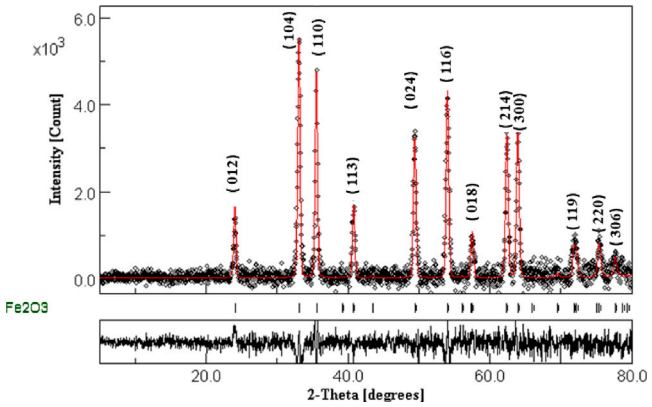

Fig. 2. Rietveld refinement analysis for α-Fe_2O_3/SiO_2 nanoparticles using MAUD. Measured XRD profile is shown by open black circles, and the calculated profile is shown by solid red line. Vertical lines represent the positions of diffraction lines for α-Fe_2O_3, and the line below the vertical lines shows the difference profile between measured and calculated patterns.

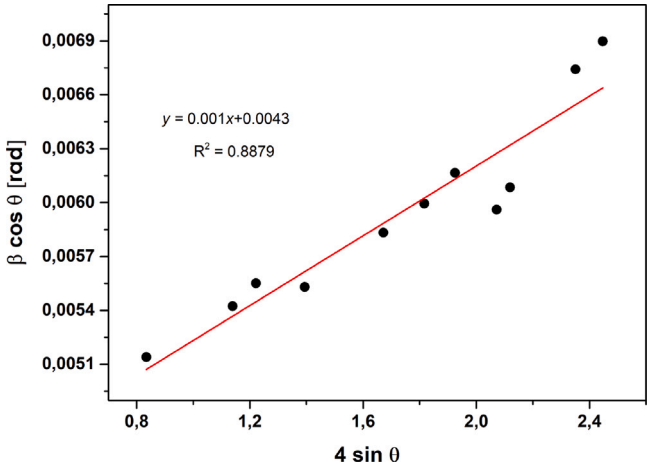

Fig. 3. Williamson–Hall plot for α-Fe_2O_3/SiO_2 nanoparticles.

due to crystallite size (β_D) can be expressed using Scherrer's equation according to:

$$\beta_D = \frac{k\lambda}{D\cos\theta} \tag{1}$$

where k is the shape factor (taken as 0.94 in this work), D is the crystallite size, and λ is the wavelength of the X-ray radiation source used.

While the broadening due to microstrain (β_ε) is known to vary in the form:

$$\beta_\varepsilon = 4\varepsilon\frac{\sin\theta}{\cos\theta} \tag{2}$$

where ε is the microstrain. And combining the two Eqs. (1) and (2) and linearizing the expression we obtain the total broadening of the peak:

$$\beta_t\cos\theta = 4\varepsilon\sin\theta + \frac{k\lambda}{D} \tag{3}$$

Hence, a graph of $\beta_t\cos\theta$ versus $4\sin\theta$ is a straight line of slope ε, enabling the microstrain and crystallite size to be determined from the slope and y-intercept (equal to $\frac{k\lambda}{D}$), respectively (see Fig. 3).

Our W–H plot results indicates that the average crystallite size of the synthesized α-Fe_2O_3 nanoparticles was 36 nm. There was a good agreement between the crystallite size obtained from MAUD and W–H plot, as expected.

Transmission electron microcopy (TEM) was used to study the particle size and morphology of the nanoparticles. A bright field TEM image

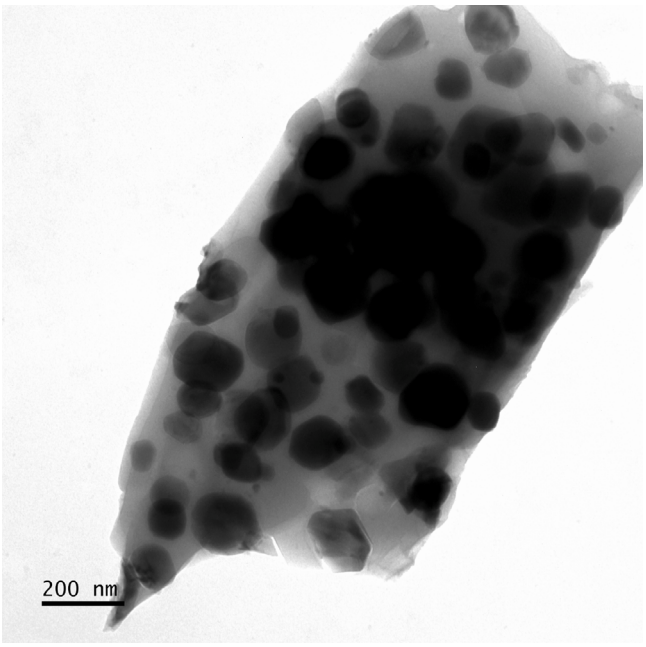

Fig. 4. Bright Field TEM micrographs of the α-Fe_2O_3/SiO_2 nanoparticles.

showing spherical nanoparticles of α-Fe_2O_3 embedded in a silica matrix is given in Fig. 4. TEM analysis showed significantly large particles as compared to crystallite size obtained from XRD analysis. An average particle size of 118 ± 28 nm was determined using Image J program (version 1.52 v). The TEM results indicates that the nanoparticles formed a "sub-particle" structure [8,24] i.e. particles composed of individual nanocrystal sub-units with size of about 36 nm. Indeed, the sample was heat treated at high annealing temperature of 1100 °C for 3 h. It is believed that this high annealing temperature favored the formation of a sub-particle structure in the sample. This argument is supported by the work of Vallina et al. [1] which demonstrated that the formation of the sub-particle structure was a consequence of the slower rate of the Scherrer crystallite size growth compared to particle size growth at high annealing temperatures.

3.2. Magnetic properties

The magnetic properties of the sample was investigated using Mössbauer spectroscopy and the vibrating sample magnetometer. Room temperature Mössbauer spectrum of α-Fe_2O_3/SiO_2 nanoparticles is reported in Fig. 5. The room temperature spectrum shows that the nanoparticles were in a magnetically ordered state as represented by the sextet. It is evident from the room temperature spectrum that there is no superparamagnetic component. Indeed, hematite only becomes superparamagnetic at critical crystallite size of 10 nm and below, and in this work the calculated crystallite size from XRD was 36 nm. Since the absence of superparamagnetic structure can be difficult to see particularly in spectra with high intensity (Fig. 5). An inset was included in the graph to show the vicinity of $v = 0$ mm/s. The inset shows no presence of a doublet, ruling out superparamagnetic behavior in the sample. The experimental Mössbauer spectrum was well fitted with just one Lorentzian sextet, and the Mössbauer parameters resulting from the fitting are reported in Table 1. The quality and reliability of the fit was monitored using the value of the goodness-of-fit χ^2. The fit yielded a χ^2 value of 1.15 ± 0.17 compared to the expected value of 1 ± 0.2. The derived Mössbauer parameters i.e. isomer shift (IS), quadrupole splitting (QS), and magnetic hyperfine field (B_{hf}), are all in good agreement with previously published Mössbauer results for hematite [3,12,18,24,36]. The isomer shift 0.37 mm/s is consistent

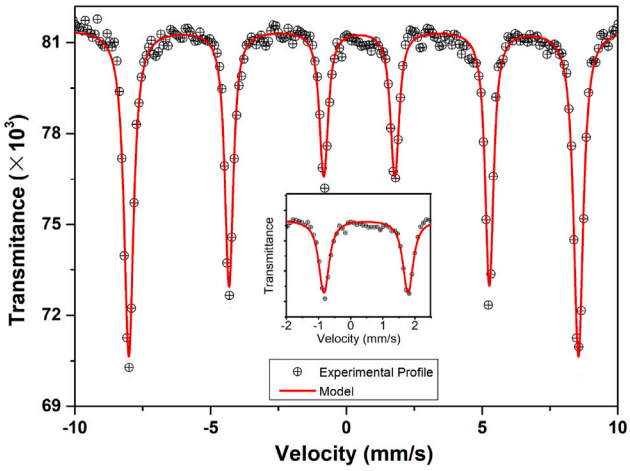

Fig. 5. Room temperature Mössbauer spectrum of α-Fe_2O_3/SiO_2 nanoparticles. Inset showing the vicinity of $\upsilon = 0$ mm/s.

Table 1
Room temperature Mössbauer fitting parameters for α-Fe_2O_3/SiO_2.

IS (mm/s)	QS (mm/s)	B_{hf} (T)	Line width (mm/s)
0.37 ± 0.01	-0.11 ± 0.01	51.3 ± 0.03	0.203 ± 0.01

with Fe^{3+} oxidation state [24]. It is noteworthy mentioning that the negative quadrupole splitting (QS) is an indication that hematite is in a weakly ferromagnetic state [24]. The Mössbauer results presented here are also in good agreement with our XRD analysis that the sample consist of only pure hematite phase without impurities.

Magnetic measurements on the sample were performed using the VSM. Isothermal $M(H)$ magnetization curves measured at 10 K & 100 K and 200 K & 300 K are reported in Figs. 6 and 7, respectively. Measurements recorded at all temperatures show open hysteresis loops. Furthermore, the $M(H)$ curves measured at 10 and 100 K exhibited small hysteresis loops compared to wide-open hysteresis loops for measurements recorded at 200 and 300 K temperature. For bulk hematite, the magnetic moments should order antiferromagnetically below T_M, and no hysteresis should be observed. However, the existence of the hysteresis loops below T_M is noted in our sample and it is attributed to uncompensated spins that exist at surface of the nanoparticles [7].

The $M(H)$ curves were observed to be slightly shifted along the H-axis. This asymmetric behavior is most of the time attributed to exchange bias (EB) effect, which manifest itself as a shift in the hysteresis loop towards the negative field after field-cooling a ferromagnet/antiferromagnet bilayers below the Néel temperature [37]. The exchange bias can be calculated from the hysteresis loop according to:

$$H_{EB} = \frac{1}{2}|H_{c1} + H_{c2}| \tag{4}$$

where H_{c1} and H_{c2} are the left (negative) and right (positive) coercivity fields, respectively.

However, detailed work on the criteria for saturated magnetization loop by Harres et al. [37] demonstrated that the asymmetric behavior which is oftenly misinterpreted as EB effect, is sometimes actually caused by the minor loop effects due to the unsaturated magnetization measurement. Since visual inspection alone is insufficient to determine whether a hysteresis loop is saturated (major) or unsaturated (minor), the procedure outlined in details in [37] and successfully applied to $SrCoO_x$ ceramics by Xie et al. [38] was followed in this work to determine the saturation of the loops. Briefly, the singular point detection (SPD) method seeks to detect singularities (i.e. a singular point where the descending and ascending branches overlap) by analyzing the successive derivatives d^nM/d^nH (where $n = 1, 2, \ldots$). A loop

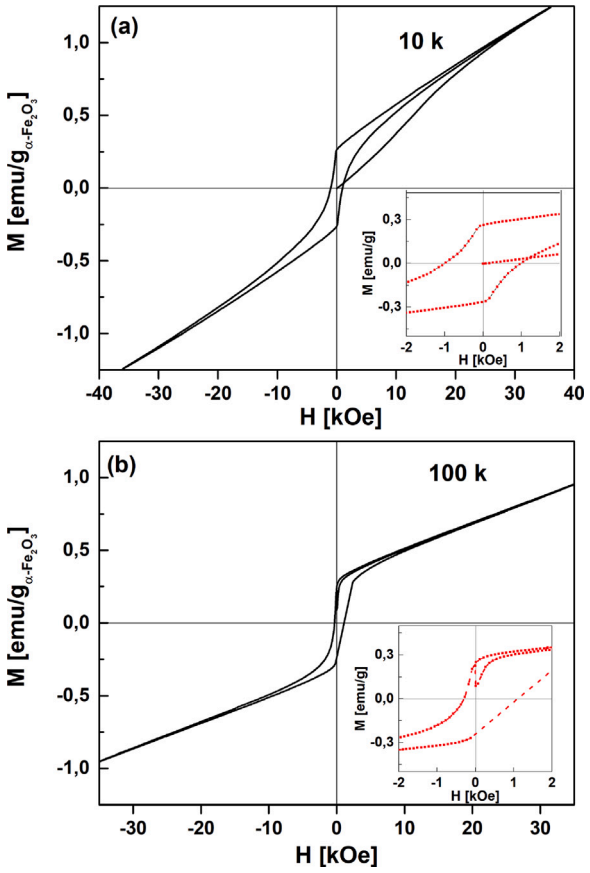

Fig. 6. M vs. H magnetization curves for α-Fe_2O_3/SiO_2 nanoparticles recorded at (a) 10 K and (b) 100 K. Insets shows low field magnetization behavior.

is then said to be saturated if such singularity exists. In this work, the derivatives dM/dH were taken and the results are reported in Fig. 9. The derivatives dM/dH of the two branches did not show a strong overlap, indicating that the hysteresis loops did not reach magnetization saturation even at the maximum applied magnetic field of 35 kOe, in agreement with our previous statement. Therefore, we can rule out EB effects in our sample and the asymmetric behavior observed is a result of minor loop effects. The coercive field H_C is then calculated according to:

$$H_C = \frac{1}{2}|H_{c1} - H_{c2}| \tag{5}$$

The room temperature magnetization curve revealed a surprisingly high coercivity of ~8.5 kOe. And a general decrease in the coercive field is observed when the sample is cooled to 10 K as illustrated in Fig. 10. The observed high H_C value at room temperature is not usual for the hematite system. In this project, a bare α-Fe_2O_3 sample was synthesized and its detailed structural analysis is reported in [32]. Here we compare the magnetic properties of the α-Fe_2O_3 sample to the hematite sample embedded in amorphous silica matrix. Presented in Fig. 8 are the field dependence magnetization curves for the bare α-Fe_2O_3 sample. Contrary to the α-Fe_2O_3/SiO_2, the bare hematite sample exhibited a small open hysteresis loop with small coercivity ~400 Oe and remnant magnetization $M_r = 0.26$ emu/g at room temperature. The observed remnant magnetization is one order of magnitude higher than reported by Vallina et al. [1], but they are in very much agreement with M_r values reported for hematite [23]. The saturation magnetization (Ms) values were then estimated from the relationship [2]:

$$M = M_s(1 - \beta/H) \tag{6}$$

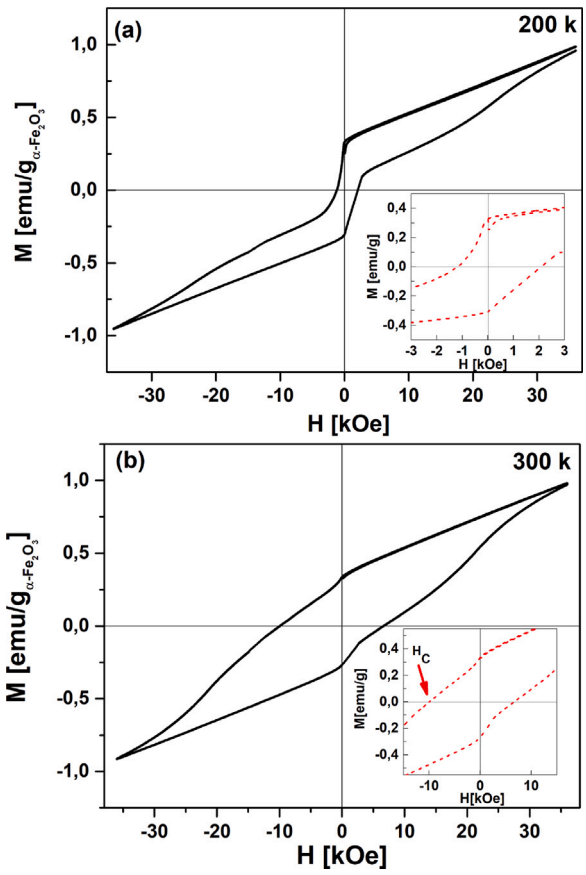

Fig. 7. M vs. H magnetization curves for α-Fe_2O_3/SiO_2 nanoparticles recorded at (a) 200 K and (b) 300 K. Insets shows low field magnetization behavior.

Table 2
Magnetic properties for α-Fe_2O_3/SiO_2 and bare α-Fe_2O_3. H_C is the coercivity, M_r is the remanent magnetization, and M_s is the saturation magnetization at 300 K (RT) and 10 K.

Sample	M_r (emu/g)	M_S (emu/g)	H_C (kOe)
α-Fe_2O_3/SiO_2	0.33 (RT) 0.27 (10 K)	1.40 (RT) 1.90 (10 K)	8.5 (RT) 1.96 (10 K)
α-Fe_2O_3	0.26 (RT) 0.22 (10 K)	1.08 (RT) 1.30 (10 K)	0.40 (RT) 0.33 (10 K)

where β is a magnetic field-independent parameter. By considering only high field data, plots of M vs. 1/H were obtained and the values of Ms were determined by extrapolating 1/H to zero field in the experimental data M vs. 1/H. The magnetic properties for the two samples are reported in Table 2. It can be noted that the saturation magnetization for our two samples is greater than M_s value of 0.3 emu/g for bulk hematite but it is smaller than Ms = 6.83 emu/g reported by Tadic et al. [7].

As mentioned before, amongst the highest coercivity for hematite (6 Koe) was reported by Rath et al. [8]. A sub-particle structure model was used in their study to explain the high H_C values in hematite, since models such as Stoner–Wohlfarth and nonmagnetic grain-boundary which are suitable to explain the dependence of H_C on dispersed particles failed to explain the observed high H_C values in their sample. It was established that their particles was in fact polycrystalline (made of a number of sub-particles). Since the sub-particles within the particles are not dispersed, it was concluded that the H_C values from such systems should be proportional to the "particle" size rather than a strong dependence on the size of their "subparticles" [8,24]. Furthermore,

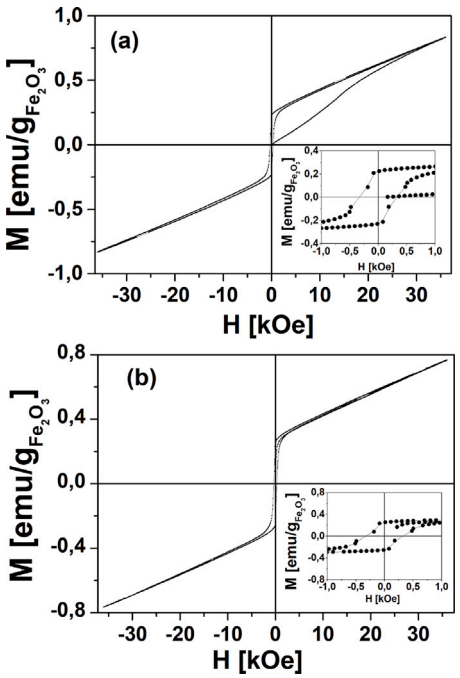

Fig. 8. Magnetization curves for bare α-Fe_2O_3 nanoparticles recorded at 10 K and 300 K. Insets shows low field magnetization behavior.

Vallina et al. [1] reported thermally-induced enhancement of magnetic coercivity for dry heated hematite samples. The authors reported an increase in magnetic coercivity (289 Oe to ~5 kOe) with increasing annealing temperature from 350 °C to 1000 °C which was attributed to the development of subparticle structure at high annealing temperatures, which is believed to permit stronger magnetic interactions. Hence, the large coercivity reported for the sample annealed at high temperature. The authors demonstrated that in the absence of the subparticle structure for sample annealed at low temperatures, hematite display low H_C values.

In our case, a discrepancy between XRD crystallite size and TEM particle size was observed. This suggests that the particles observed by TEM was made of a number of small crystallites, the sub-particles. Therefore, the number of sub-particles inside the particle and their interaction is believed to be responsible for this rather unusually high H_C value observed in this study, in agreement with Rath et al. [8] and Vallina et al. [1]. In fact, the α-Fe_2O_3 sample investigated in this current study was annealed slightly above 1000 °C, the annealing temperature which displayed the highest coercivity from the four hematite samples reported by Vallina et al. [1]. Furthermore, the observed high H_C value in this study could not have resulted from the presence of the ε-Fe_2O_3 phase which is known to have high H_C values. Firstly, both our XRD and Mossbauer spectroscopy studies ruled out the presence of any impurity phase. Secondly, according to Nikolić et al. [4], the temperature 1060 °C was observed to be a threshold temperature for the ε-Fe_2O_3 stability, above which the ε-Fe_2O_3 phase disappears. Our sample was annealed at 1100 °C, just above the threshold temperature, ruling out the presence of the ε-Fe_2O_3 phase in our sample. Therefore the observed high H_C value is purely from the α-Fe_2O_3 phase and it is attributed to the formation of sub-particle structure at 1100 °C.

Origins of Coercivity in hematite

It has been well established that coercivity in magnetic systems originates from intrinsic magnetocrystalline anisotropy, stress-induced magnetoelastic anisotropy, and shape anisotropy [39]. Because of its weak magnetization, the main source of high coercivity for both fine and large hematite particles has been attributed to magnetoelastic anisotropy as both magnetocrystalline and shape anisotropies are

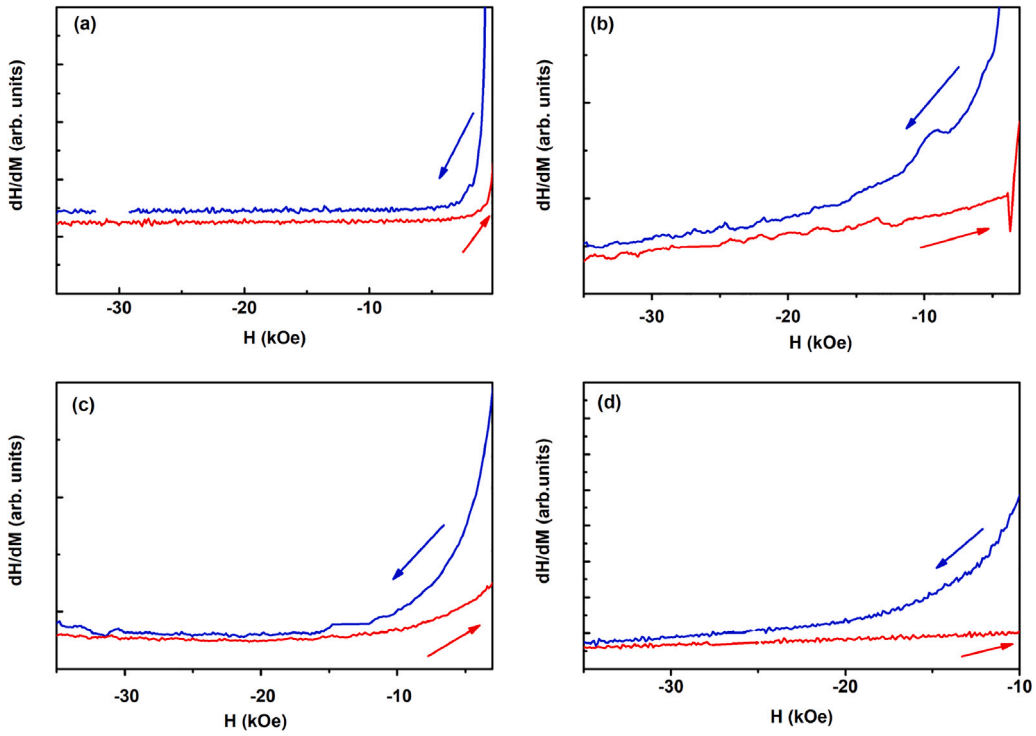

Fig. 9. Derivatives M vs. H magnetization curves for α-Fe_2O_3/SiO_2 nanoparticles recorded at (a) 10 K, 100 K, 200 K and (b) 300 K. The blue and red arrows indicates the descending and ascending branches, respectively.

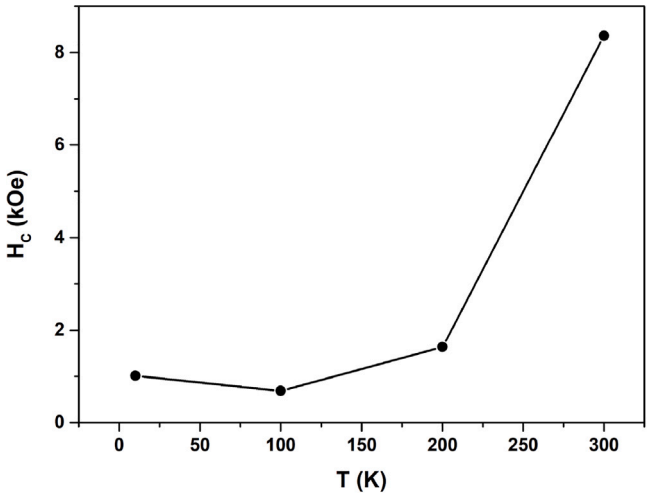

Fig. 10. Coercivity as a function of temperature for α-Fe_2O_3/SiO_2.

deemed inadequate [40,41]. Indeed, we can rule out the contribution of shape anisotropy in our sample since TEM measurements showed particles with mostly spherical morphology. For shape anisotropic particles, coercivity increases with increase of aspect ratio. Therefore, spherical particles with aspect ratio ~1, exhibit no net shape anisotropy [9].

Grain-size dependent trends: Özdemir and Dunlop [41] studied the particle size dependence of H_C on a number of submicron hematites with particles sizes 0.12 – 0.45 μm. A plot of H_C vs. grain size for different hematites displayed an interesting pattern which was modeled by a polynomial function. At first, H_C increases rapidly with increasing particle size until it reaches a maximum for particle size between 0.1 – 3 μm, and then a steadily decreasing trend was observed upon further increase in particle size. It is worth mentioning that the particle size of 118 nm (0.118 μm) for the sample investigated in this work is well within the particle sizes at which the coercivity of hematite is reported to reach maximum by Özdemir and Dunlop [41].

Thermal-treatment trends: The strong dependence of magnetic properties of hematite, particularly coercivity, on annealing treatment is well documented in literature e.g. Dekkers [42] reported an increase in coercivity in hematite samples by several thousands Oe after heat treatment, Zysler et al. [13] observed an increase in coercivity with thermal treatment (H_C). Magnetic measurements recorded at room temperature by Vallina et al. [1] displayed a strong synthesis-temperature dependency on the coercivity mechanism of hematite. In that report, narrow hysterersis loops at 350 °C to wide-open loops at 1000 °C were observed, indicating the strong dependency of coercivity on synthesis-temperature. It is noteworthy to mention that the sample under investigation in this work was heat treated at 1100 °C, a synthesis-temperature close to that annealing temperature where Vallina et al. [1] recorded the highest coercivity.

Role of Silica in enhancing coercivity: As demonstrated using the α-Fe_2O_3/SiO_2 sample, the hematite nanoparticles embedded in silica displayed an enhanced coercive field compared to the bare α-Fe_2O_3 sample. The enhancement of H_C as a result of coating hematite nanoparticles with silica has been observed before e.g. Reufer et al. [26] and Tadic et al. [7] reported an increase in H_C for silica coated hematite nanoparticles. However, the silica coating did not seem to have any influence on the remnant magnetization as it remained unchanged for the α-Fe_2O_3/SiO_2 and bare α-Fe_2O_3 samples, which is consistent with the observation in [26].

The role of silica in enhancing the coercivity in hematite nanoparticles could be explained by its role in influencing magnetic interparticle interaction (IPI). It is known that the magnetism of magnetic nanoparticles is strongly influenced by magnetic interparticle interactions i.e. dipole–dipole interaction (long range) and exchange interaction (short range) [43,44]. It is well established that one of the features of magnetic IPI is the shift of the superparamagnetic blocking temperatures (T_B) to higher temperatures [44,45]. For the hematite system, it was previously reported that the silica coating reduces T_B in hematite nanoparticles [26]. This indicates that the role of silica

is to minimize magnetic IPI in hematite, because if magnetic IPI was present, it was expected to increase T_B. Silica, being a non-magnetic inert oxide, reduces the direct dipole–dipole interaction between particles, thereby enhancing the coercivity. Indeed, interparticle dipolar interactions reduces the energy barrier to magnetic reversal and consequently decreases the coercivity in interacting particles compared to non-interacting particles [46]. This is because in non-interacting magnetic particles, the isolated particles can reverse their magnetization individually without influencing the neighboring magnetic particles [7]. This isolated magnetic behavior may enhance coercivity because a strong field will be required to reverse the magnetization of each individual particle.

On the other hand, our TEM and XRD analysis revealed that the well-defined particles observed by TEM are in fact polycrystalline i.e. aggregates of nanocrystalline subparticles. For such multigranular nanostructures, the short range intraparticle dipolar interactions between the subparticles becomes significant [7,47]. The microstructure-dependent magnetic properties of hematite are reported by Tadic et al. [7] and Vallina et al. [1]. They show that strong magnetic interactions between nanocrystal sub-units i.e. intraparticle interactions results in enhanced coercivity in hematite. This is because these interactions may increase the effective magnetic anisotropy which effectively enhances the coercivity [7]. Das et al. [47] also reported an increase in the anisotropy field for iron oxide nanoparticles due to Intraparticle interactions. Since magnetic anisotropy is linked to coercivity, an increase in magnetic anisotropy would imply an increase in coercive field. Therefore, the unusually high value of H_C results in our sample could be attributed to the strong intraparticle magnetic interactions in the nanoparticles due to formation of the subparticle structure.

Measurement-Temperature Dependence of Coercivity

Magnetization measurements at different temperatures for the α-Fe_2O_3 sample investigated in this work displayed a strong dependence of the coercive field on measurement temperature. H_C values were shown to increase with increasing temperature as illustrated in Fig. 10, this behavior is rather unusual for magnetic minerals. In most typical magnetic systems, coercivity is known to increase with decreasing temperature [48,49] since an increase in coercivity is related to an increase in the anisotropy field [7]. This field generally increases with decreasing temperature. However, anomalous coercivity dependence on temperature where H_C increases with increasing temperature has been reported before e.g. for calcined $BiFeO_3$ ferrite, H_C were observed to linearly increase with increasing temperature [50]. Rong et al. [51] and Ahmmad etal. [52] also reported anomalous coercive Fields that increased with increasing temperature in SmCo-based magnets and multiferroic systems, respectively. Increase of coercivity with increasing temperature has also been previously observed for hematite nanoparticles e.g. Tadic et al. [7] reported a coercivity of 160 Oe at 5 K compared to 4.350 kOe at 300 K for hematite. For polycrystalline nanopowders, the temperature dependence of coercivity can be expressed by the phenomenological formula [50,51,53]:

$$\mu_0 H_C = \alpha_{ex}\alpha_k \mu_0 H_a - N_{eff} J_s \quad (7)$$

where α_k is the Kronmuller parameter which describes the influence of the non-perfect surface of the particles on the magnetocrystalline anisotropy, the microstructural parameter α_{ex} takes into account the effect of the exchange coupling between neighboring grains, N_{eff} is the magnetostatic interaction parameter due to enhanced stray fields at the edges and corners of the particles, H_a is the anisotropy field, and J_s is the magnetization. Anomalous coercivity mechanism i.e. increase in H_C with increasing temperature is observed in granular systems if the interparticle coupling decreases with temperature [50,51]. The exact coercivity mechanism for this sample is not known and should be a subject of further investigations, but it is reasonable that the observed reduction in coercivity at low temperatures for the sample as compared to room temperature H_C value could be explained by the coercivity mechanism described in [50,51]. For nanopowders, intergranular coupling is weak and it is further suppressed by an increase in temperature [50]. Furthermore, the sample was coated with silica, which also played an important role in further suppressing the intergranular coupling. Hence an increase in coercivity with increasing temperature (10 K to 300 K) was observed for the silica coated sample.

4. Conclusion

Transmission electron microscopy analysis for the α-Fe_2O_3/SiO_2 sample showed an average particle size of ≈118 nm of roughly spherical shaped nanoparticles embedded in silica matrix. The room temperature Mössbauer spectra confirmed a magnetically ordered state for this sample with Mössbauer parameters consistent with hematite. Hysteresis loops at 300 K showed an unusually high coercivity of H_C ~8.5 kOe and remanent magnetization of about 0.25 emu/g. According to our knowledge, no such high coercivity value for hematite was reported before. This was explained using sub-particle structure formation of nanoparticles in the sample. It is believed that this single high temperature heating resulted in a sub-particle structure formation which resulted in the observed high coercivity.

Another remarkable feature observed about the α-Fe_2O_3 sample was that its coercivity was found to increase with temperature, where $M(H)$ curves exhibited smaller coercivities at 10 K than at 300 K. This anomalous coercivity mechanism was attributed to the reduction in interparticle exchange coupling on increasing temperature.

CRediT authorship contribution statement

C.J. Masina: Writing – original draft, Supervision, Project administration, Conceptualization. **A.E. Chithwayo:** Investigation. **T. Moyo:** Formal analysis. **S. Dlamini:** Data curation. **D. Wamwangi:** Writing – review & editing, Data curation.

Declaration of competing interest

The authors declare the following financial interests/personal relationships which may be considered as potential competing interests: Colani Masina reports equipment, drugs, or supplies was provided by University of the Witwatersrand Johannesburg. If there are other authors, they declare that they have no known competing financial interests or personal relationships that could have appeared to influence the work reported in this paper.

Data availability

Data will be made available on request.

Acknowledgments

The financial support from the School of Chemistry and Physics UKZN and the National Research Foundation (NRF), South Africa, is acknowledged. Daniel Wamwangi would like to thank financial support through the National Equipment Program of the NRF (grant: UID: 116181).

References

[1] B. Vallina, J.D. Rodriguez-Blanco, A.P. Brown, L.G. Benning, J. Blanco, Enhanced magnetic coercivity of α–Fe_2O_3 obtained from carbonated 2-line ferrihydrite, J. Nanopart. Res. 16 (2322) (2014) 1–13.

[2] M. Tadic, M. Panjan, B.V. Tadic, J. Lazovic, V. Damnjanovic, M. Kopani, L. Kopanja, Magnetic properties of hematite (α-Fe_2O_3) nanoparticles synthesized by sol-gel synthesis method: The influence of particle size and particle size distribution, J. Electr. Eng. 70 (2019) 71–76.

[3] J. Jacob, M. AbdulKhadar, VSM and Mössbauer study of nanostructured hematite, J. Magn. Magn. Mater. 322 (2009) 614–621.

[4] V.N. Nikolić, M. Tadić, M. Panjan, L. Kopanja, N. Cvjetićanin, V. Spasojević, Influence of annealing treatment on magnetic properties of Fe_2O_3/ SiO $_2$ and formation of ε-Fe_2O_3 phase, Ceram. Int. 43 (2017) 3147–3155.

[5] D. Kubániová, L. Kubíčková, T. Kmječ, K. Závěta, D. Nižňanský, P. Brázda, M. Klementová, J. Kohout, Hematite: Morin temperature of nanoparticles with different size, J. Magn. Magn. Mater. 475 (2019) 611–619.

[6] C. Powell, A. Lounsbury, Z.S. Fishman, C.L. Cooorod, M.J. Gallagher, D. Villagran, J.B. Zimmerman, L.D. Pfefferle, M.S. Wong, Nano-structural effects on hematite (α-Fe_2O_3) nanoparticle radiofrequency heating, Nano Converg. 23 (2021) 3255–3272.

[7] M. Tadic, N. Citakovic, M.P.B. Stanojevic, D. Markovic, D. Jovanovic, V. Spasojevic, Synthesis, morphology and microstructure of pomegranate-like hematite (α-Fe_2O_3) superstructure with high coercivity, J. Alloys Compd. 543 (2012) 118–124.

[8] C. Rath, K.K. Sahu, S.D. Kulkarni, S. Anand, S.K. Date, R.P. Das, N.C. Mishra, Microstructure-dependent coercivity in monodispersed hematite particles, Appl. Phys. Lett. 75 (1999) 4171–4173.

[9] M.T.N. Čitaković, M. Panjan, Z. Stojanović, D.M.V. Spasojević, Synthesis, morphology, microstructure and magnetic properties of hematite submicron particles, J. Alloys Compd. 509 (2011) 7639–7644.

[10] M. Tadic, V. Kusigerski, D. Markovic, I. Milosevic, V. Spasojevic, High concentration of hematite nanoparticles in a silica matrix: structural and magnetic properties, J. Magn. Magn. Mater. 321 (2009) 12–16.

[11] L. Kopanja, I. Milosevic, M. Panjan, D. Damnjanovic, M. Tadic, Sol–gel combustion synthesis, particle shape analysis and magnetic properties of hematite (α-fe2o3) nanoparticles embedded in an amorphous silica matrix, Appl. Surf. Sci. 362 (2016) 380–386.

[12] R.M. Cornell, U. Schwertmann, The iron oxides: structureand propertiesand reactionsand occurrences and uses, 2003.

[13] R.D. Zysler, M. Vasquez-Mansilla, C. Arciprete, M. Dimitrijewits, D. Rodriguez-Sierra, C. Saragovi, Structure and magnetic properties of thermally treated nanohematite, J. Magn. Magn. Mater. 224 (2001) 39–48.

[14] A. Abrajevitch, A.P. Roberts, B.J. Pillans, R.S. Horie, Unexpected magnetic behavior of natural Hematite-Bearing Rocks at low temperatures, Geochem. Geophys. 22 (2021) 1–11.

[15] L. Machala, J. Tuček, R. Zboříl, Polymorphous transformations of nanometric iron(III) oxide: A review, Chem. Mater. 23 (2011) 3255–3277.

[16] D. Kubániová, L. Kubíčková, T.K.K. Závěta, D. Nižňanský, P. Brázda, M. Klementová, J. Kohout, Hematite: Morin temperature of nanoparticles with different size, J. Magn. Magn. Mater. 475 (2019) 611–619.

[17] Ö. Özdemir, D.J. Dunlop, T.S. Berquó, Morin transition in hematite: Size dependence and thermal hysteresis, Geochem. Geophys. Geosyst. 9 (10) (2008) 1–12.

[18] F. Bødker, M.F. Hansen, C.B. Koch, K. Lefmann, S. Mørup, Magnetic properties of hematite nanoparticles, Phys. Rev. B 61 (2000) 6826–6838.

[19] I. Dzyaloshinsky, A thermodynamic theory of "weak" ferromagnetism of antiferromagnetics, J. Phys. Chem. Solids 4 (1958) 241–255.

[20] D.J. Dunlop, Ö. Özdemir, Rock Magnetism: Fundamentals and Frontiers, vol. 3, Cambridge University Press, 2001.

[21] J. Svoboda, Magnetic methods for the treatment of minerals, Magn. Sep. News 2 (1987) 223–224.

[22] D.J. Dunlop, Magnetic properties of fine-particle hematite, Ann. Geophys. 27 (1971) 269–293.

[23] M.M. Rafi, K.S.Z. Ahmed, K.P. Nazeer, D.S. Kumar, M. Thamilselvan, Synthesis, characterization and magnetic properties of hematite (α-Fe_2O_3) nanoparticles on polysaccharide templates and their antibacterial activity, Appl. Nanosci. 5 (2015) 515–520.

[24] P.G. Bercoff, H.R. Bertorello, Magnetic properties of hematite with large coercivity, Appl. Phys. A Mater. Sci. Process. 100 (2010) 1019–1026.

[25] N.K. Chaudhari, H.C. Kim, C.S. Kim, J. Park, J. Yu, Solvent controlled synthesis of new hematite superstructures with large coercive values, CrystEngComm 14 (2012) 2024–2031.

[26] M. Reufer, H. Dietsch, U. Gasser, B. Grobety, A.M. Hirt, V.K. Malik, P. Schurtenberger, Magnetic properties of silica coated spindle-type hematite particles, J. Phys.: Condens. Matter. 23 (2011) 065102.

[27] J. Tuček, J. Zbořil, A. Namai, S. Ohkoshi, ε-Fe_2O_3: An advanced nanomaterial exhibiting giant coercive field, millimeter-wave ferromagnetic resonance, and magnetoelectric coupling, Chem. Mater. 22 (2010) 6483–6505.

[28] L. Machalaand, J. Tuček, R. Zbořil, Polymorphous transformations of nanometric Iron(III) Oxide: A review, Chem. Mater. 23 (2011) 3255–3272.

[29] M. Gich, A. Roig, C. Frontera, E. Molins, J. Sort, M. Popovici, G. Chouteau, D.M. y Marero, J. Nogués, Large coercivity and low-temperature magnetic reorientation in ε-Fe_2O_3 nanoparticles, Chem. Mater. 23 (2011) 3255–3272.

[30] J. García-Muñoz, A. Romaguera, F. Fauth, J. Nogués, M. Gich, Unveiling a new high-temperature ordered magnetic phase in ε-Fe_2O_3, Chem. Mater. 29 (22) (2017) 9705–9713.

[31] J. Zhang, L.X. Rong, Y. Liu, B.Z. Dong, SAXS study on the microstructure of Fe_2O_3 nanocrystal, Mater. Sci. Eng. A 351 (2003) 224–227.

[32] A.E. Chithwayo, The Synthesis and Characterization of Magnetic α-Fe_2O_3 and ε-Fe_2O_3 phase Nanoparticles (Msc Dissertation), University of Kwa-Zulu Natal, South Africa, 2021.

[33] T. Dannegger, A. Deák, L. Rózsa, E. Galindez-Ruales, S. Das, E. Baek, Magnetic properties of hematite revealed by an ab initio parameterized spin model, Phys. Rev. B 107 (2023) 184426.

[34] I.A. Al-Omari, V. Narayanaswamy, S. Halder, H.H. Hamdeh, S. Alaabed, A.S. Kamzin, C.V.V.M. Gopi, A. Khaleel, B. Issa, I.M. Obaidat, Mossbauer investigations in hematite nanoparticles, Biointerface Res. Appl. Chem. 12 (2022) 4625–4636.

[35] E.H. Kisi, Rietveld analysis of powder diffraction patterns, Mater. Forum 18 (1994) 135–153.

[36] E. Murad, Properties and behavior of Iron Oxides as determined by Mössbauer spectroscop, in: J.W. Stuckiand, B.A. Goodmanand, U. Schwertmann (Eds.), Iron in Soils and Clay Minerals, 1988, pp. 309–350.

[37] A. Harres, M. Mikhov, V. Skumryev, A.M.H. de Andrade, J.E. Schmidt, J. Geshev, Criteria for saturated magnetization loop, J. Magn. Magn. Mater. 402 (2016) 76–82.

[38] L. Xie, H.L. Huang, Y.L. Lu, Temperature- and magnetic fielddependence of exchange bias in $srcoo_{2.29}$ ceramics, AIP Adv. 7 (2017) 015207–1–015207–7.

[39] Q. Liu, V. Barrón, J.T.H. Qin, Y. Yu, The magnetism of micro-sized hematite explained, Phys. Earth Planet. Inter. 183 (2010) 387–397.

[40] D.J. Dunlop, K.S. Argyle, Thermoremanence, anhysteretic remanence and susceptibility of submicron magnetites: Nonlinear field dependence and variation with grain size, J. Geophys. Res. 102 (1997) 20199–20210.

[41] Ö. Özdemir, D. Dunlop, Hysteresis and coercivity of hematite, Geophys. Res.: Solid Earth 119 (2014) 2582–2594.

[42] M.J. Dekkers, Some Rockmagnetic Parameters for Natural Goethite, Pyrrhotite and Fine-Grained Hematite (Ph.D. thesis), University of Utrecht, 1988.

[43] K. Nadeem, H. Krenn, T. Traussnig, R. W^{f}urschum, D.V. Szabó, I. Letofsky-Papst, Effect of dipolar and exchange interactions on magnetic blocking of maghemite nanoparticles, J. Magn. Magn. Mater. 50 (2017) 199–202.

[44] D.A. Balaev, S.V. Semenov, A.A. Dubrovskiy, S.S. Yakushkin, V.L. Kirillov, O.N. Martyanov, Superparamagnetic blocking of an ensemble of magnetite nanoparticles upon interparticle interactions, J. Magn. Magn. Mater. 50 (2017) 199–202.

[45] Y.V. Knyazev, D.A. Balaev, S.A. Skorobogatov, D.A. Velikanov, A. Bayukov, S.V. Stolyar, R.N. Yaroslavtsev, R.S. Iskhakov, Spin dynamics in ensembles of ultrafine ferrihydrite nanoparticles, Phys. Rev. B 107 (2023) 115413s.

[46] S.N. Trukhan, O.N. Martyanov, V.F. Yudanov, Stepwise magnetization of dispersed ferromagnets due to magnetic interparticle interactions, Phys. Solid State 50 (2008) 456–462.

[47] R. Das, J.A. Masa, V. Kalappattil, Z. Nemati, I. Rodrigo, E.G. 6, J. García, M. Phan, H. Srikanth, Iron oxide nanorings and nanotubes for magnetic hyperthermia: The problem of intraparticle interactions, Nanomaterials 11 (2021) 1380.

[48] X.H. Huang, J.F. Ding, G.Q. Zhang, Y. Hou, Y.P. Yao, X.G. Li, Size-dependent exchange bias in $La_{0.25}Ca_{0.75}MnO_3$ nanoparticles, Phys. Rev. B 78 (2008) 224408–1–224408–5.

[49] T.J. Park, G.C. Papaefthymiou, A.J. Viescas, Y. Lee, H. Zhou, S.S. Wong, Composition-dependent magnetic properties of $BiFeO_3$-$BaTiO_3$ solid solution nanostructures, Phys. Rev. B 82 (2010) 024431.

[50] I. Szafraniak-Wiza, B. Andrzejewski, B. Hilczer, Magnetic properties of bismuth ferrite nanopowder obtained by mechanochemical synthesis, Acta Phys. Pol. A 126 (2014) 1029–1031.

[51] C. Rong, H. Zhang, B. Shen, J.P. Liu, Mechanism of the anomalous temperature dependence of coercivity in Sm(Co,Fe,Cu,Zr)z high-temperature magnets, Appl. Phys. Lett. 88 (2006) 042504.

[52] B. Ahmmad, M.Z. Islam, A. Billah, M.A. Basith, Anomalous coercivity enhancement with temperature and tunable exchange bias in Gd and Ti co-doped $BiFeO_3$ multiferooids, J. Phys. D: Apply. Phys. 49 (2016) 095001–1–095001–7.

[53] D. Goll, M. Seeger, H. Kronmuller, Magnetic and microstructural properties of nanocrystalline exchange coupled PrFeB permanent magnets, J. Magn. Magn. Mater. 185 (1998) 49–60.